Nonlinear Flutter of Two-Dimensional Simply Supported Symmetric Composite Laminated Plates

Le-Chung Shiau* and Li-Teh Lu†
National Cheng Kung University, Tainan, Taiwan 70101, Republic of China

The nonlinear flutter behavior of a two-dimensional simply supported symmetric composite laminated plate at high supersonic Mach number has been investigated. Von Karman's large deflection plate theory and quasisteady aerodynamic theory have been employed. Galerkin's method has been used to reduce the governing equations to a system of nonlinear ordinary differential equations in time, which are then solved by a direct numerical integration method. Nonlinear flutter results are presented with the effects of aerodynamic damping, in-plane force, static pressure differential, and anisotropic properties. Results show that the anisotropic properties such as fiber orientation and elastic modulus ratio have significant effects on the behavior of both limit cycle oscillation and chaotic motion.

Introduction

BECAUSE of their superior strength-to-weight and stiffness-to-weight ratios, as compared with conventional materials, composite materials have been widely used in aeronautical industries to replace metal in the aircraft structures for the purpose of weight saving. To use them efficiently, a good understanding of their structural and dynamic behaviors under various loads is needed. At the current stage, in high-performance military aircraft, composite materials are mostly used to make skin of wings and fuselage of an aircraft. Hence, laminated plates are of particular interest. During high-speed flight, the external skin panel of an airframe may exhibit flutter. Panel flutter is a self-excited oscillation and is due to dynamic instability of inertia, elastic, and aerodynamic forces of the system. Linear structural theory indicates that there is a critical dynamic pressure above which the panel motion becomes unstable and grows exponentially with time. However, with large amplitude oscillations, the in-plane tensile stresses induced by the geometrically nonlinear effects will restrain the panel motion to a bonded value with increasing amplitude as dynamic pressure increases. Hence, the linear theory can only determine the flutter boundary and cannot give any information about the flutter oscillation itself. For a more thorough understanding and more realistic assessment of the panel flutter problems, the geometrically nonlinear effect due to large amplitude oscillations should be considered.

In the past 30 years, different approaches have been used to study the nonlinear flutter behavior of isotropic panels. Galerkin's method with direct numerical integration was employed by Dowell[1,2] and Ventres and Dowell[3] to study two- and three-dimensional nonlinear flutter of isotropic panels. Their results show that the aerodynamic damping, in-plane forces, and static pressure differentials have significant effect on the flutter behavior of the plate. Some researchers[4-7] later on used harmonic balance method and perturbation method to determine the characteristics of the limit cycle oscillations, and results obtained for two- and three-dimensional problems agree well with those obtained by direct integration method. Because of its versatile applicability, a finite element technique was employed by several researchers[8-11] in the late 1970s and early 1980s to study the nonlinear panel flutter problems of two- and three-dimensional isotropic plates. However, the solutions were limited to harmonic of limit cycle oscillation. In 1982, Dowell[12] pointed out that in the presence of in-plane compressive loads the limit cycle oscillation may become chaotic motion in a certain range of aerodynamic pressure. Hence, assuming the flutter motion of the panel is harmonic may not lead to correct results for certain cases.

For panels made of advanced composite materials, the flutter characteristics are still not well defined, and very limited literature on this subject has appeared in journals, especially for the case of nonlinear flutter. In 1967, Ketter[13] used the Rayleigh-Ritz method to study the flutter of orthotropic panels with various boundary conditions. With panel aspect ratio = 3, his results show that the highest flutter boundaries fall in the vicinity of a filament angle of 30 deg for all boundary conditions. In 1974, Rossettos and Tong[14] analyzed the flutter of cantilever anisotropic plates by a finite element method, and the results indicate a generally strong lack of monotonic dependence on filament angle. More detailed studies about the linear flutter behavior of composite laminated plates were performed in Refs. 15 and 16 using either Galerkin's method or a finite element method. Effects of fiber orientation, stacking sequency, anisotropic property, aspect ratio, and flow angularity were considered in their analyses, and results show that anisotropic properties have significant effect on the flutter boundaries.

In this paper, Galerkin's method coupled with a direct numerical integration technique is used to study the nonlinear flutter behavior of a two-dimensional simply supported symmetric composite laminated plate exposed to supersonic flow. Von Karman's large deflection plate theory and quasisteady aerodynamic theory are employed for the analysis. The effects of composite filament angle and orthotropic modulus ratio on the flutter behavior of the composite plate are examined. Results are presented for limit cycle oscillation and chaotic motion as functions of fiber orientation, modulus ratio, dynamic pressure, inplane load, static pressure differential, and mass ratio.

Equation Formulations

Consider a two-dimensional thin plate with length a, thickness h, and mass density per unit volume ρ_m, as shown in Fig. 1. The plate is assumed to consist of K layers of homogeneous anisotropic sheets bonded together. Each layer has arbitrary elastic properties and fiber orientation but the laminate stacking sequence is symmetrical about the midplane of the plate. Supersonic airflow with air density ρ, flow velocity U, Mach

Received Oct. 2, 1989; revision received Aug. 1, 1990; accepted for publication Nov. 9, 1990.

*Visiting Professor, Institute of Aeronautics and Astronautics.
†Graduate Student, Institute of Aeronautics and Astronautics.

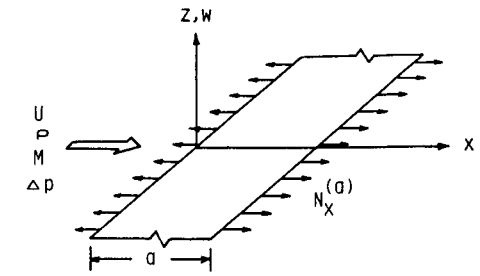

a) Plate configuration

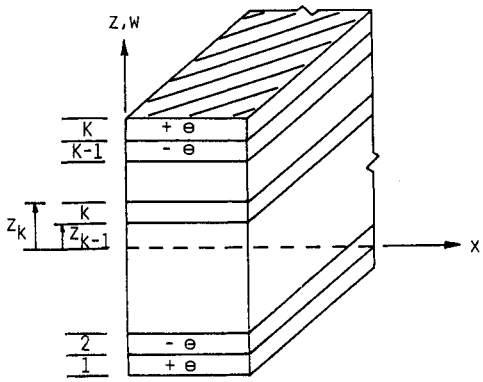

b) Ply stacking sequence

Fig. 1 Plate geometry and ply stacking sequence.

number M, and aerodynamic pressure Δ_p is assumed passing over the top surface of the plate along the positive x direction. The plate is also subjected to an applied in-plane load $N_x^{(a)}$ and a geometrically nonlinear induced in-plane force $N_x^{(i)}$. In addition, there is a static pressure differential P_s across the plate.

The differential equation of motion for a general symmetric composite plate with large oscillations can be described by von Karman's large deflection plate theory[17] as

$$D_{11}\frac{\partial^4 w}{\partial x^4} + 4D_{16}\frac{\partial^4 w}{\partial x^3 \partial y} + 2(D_{12} + 2D_{66})\frac{\partial^4 w}{\partial x^2 \partial y^2} + 4D_{26}\frac{\partial^4 w}{\partial x \partial y^3} + D_{22}\frac{\partial^4 w}{\partial y^4} - \left\{\frac{\partial u^\circ}{\partial x} + \frac{1}{2}\left(\frac{\partial w}{\partial x}\right)^2\right\} \times \left(A_{11}\frac{\partial^2 w}{\partial x^2} + 2A_{16}\frac{\partial^2 w}{\partial x \partial y} + A_{12}\frac{\partial^2 w}{\partial y^2}\right) - \left(\frac{\partial u^\circ}{\partial y} + \frac{\partial v^\circ}{\partial x} + \frac{\partial w}{\partial x}\frac{\partial w}{\partial y}\right)\left(A_{16}\frac{\partial^2 w}{\partial x^2} + 2A_{66}\frac{\partial^2 w}{\partial x \partial y} + A_{26}\frac{\partial^2 w}{\partial y^2}\right) - \left\{\frac{\partial v^\circ}{\partial y} + \frac{1}{2}\left(\frac{\partial w}{\partial y}\right)^2\right\}\left(A_{12}\frac{\partial^2 w}{\partial x^2} + 2A_{26}\frac{\partial^2 w}{\partial x \partial y} + A_{22}\frac{\partial^2 w}{\partial y^2}\right) + \rho_m h\frac{\partial^2 w}{\partial t^2} + \Delta p = P_s \quad (1)$$

where u°, v°, w are the midplane displacements in the x, y, z directions, respectively. D_{ij} and A_{ij} are the plate bending and extensional rigidities, respectively, and are defined as

$$D_{ij} = \frac{1}{3}\sum_{k=1}^{K}\overline{Q}_{ij}^{(k)}(z_k^3 - z_{k-1}^3) \qquad (i, j = 1, 2, 6) \quad (2)$$

$$A_{ij} = \sum_{k=1}^{K}\overline{Q}_{ij}^{(k)}(z_k - z_{k-1}) \qquad (i, j = 1, 2, 6) \quad (3)$$

where $\overline{Q}_{ij}^{(k)}$ is the transformed reduced stiffnesses.[18]

Equation (1) can be reduced to an equation of motion for a two-dimensional composite plate (infinite long in the y direction as shown in Fig. 1) by deleting all terms involving y and v°

$$D_{11}\frac{\partial^4 w}{\partial x^4} - [N_x^{(a)} + N_x^{(i)}]\frac{\partial^2 w}{\partial x^2} + \rho_m h\frac{\partial^2 w}{\partial t^2} + \Delta p = P_s \quad (4)$$

where

$$N_x^{(a)} = A_{11}\frac{\partial u^\circ}{\partial x} \quad (5)$$

$$N_x^{(i)} = \frac{1}{2}\frac{A_{11}}{a}\int_0^a \left(\frac{\partial w}{\partial x}\right)^2 dx \quad (6)$$

For high Mach numbers ($M > 1.6$), the aerodynamic pressure loading Δp is assumed to follow two-dimensional quasisteady supersonic aerodynamic theory:

$$\Delta p = \frac{\rho U^2}{\sqrt{M^2 - 1}}\left[\frac{\partial w}{\partial x} + \frac{M^2 - 2}{M^2 - 1}\frac{1}{U}\frac{\partial w}{\partial t}\right] \quad (7)$$

Introducing the following nondimensional parameters and constants

$$W = w/h, \qquad \xi = x/a$$

$$\tau = t\sqrt{\frac{D_{11}^{(0)}}{\rho_m h a^4}}, \qquad \mu = \frac{\rho a}{\rho_m h}$$

$$R_x = \frac{N_x^{(a)}a^2}{D_{11}^{(0)}}, \qquad \lambda = \frac{\rho U^2 a^3}{\sqrt{M^2 - 1}D_{11}^{(0)}}, \qquad P = \frac{P_s a^4}{D_{11}^{(0)}h} \quad (8)$$

Equations (4–7) can be nondimensionalized and combined into one equation as

$$\frac{D_{11}}{D_{11}^{(0)}}\frac{\partial^4 W}{\partial \xi^4} - \frac{A_{11}h^2}{2D_{11}^{(0)}}\left\{\int_0^1 \left(\frac{\partial W}{\partial \xi}\right)^2 d\xi\right\}\frac{\partial^2 W}{\partial \xi^2} - R_x\frac{\partial^2 W}{\partial \xi^2} + \frac{\partial^2 W}{\partial \tau^2} + \lambda\left[\frac{\partial W}{\partial \xi} + \left(\frac{\mu}{\lambda M}\right)^{1/2}\frac{\partial W}{\partial \tau}\right] = P \quad (9)$$

where

$$D_{11}^{(0)} = \frac{h^3 E_1^2}{12(E_1 - \nu_{12}^2 E_2)}$$

is the value of D_{11} when all fibers are aligned with the x axis and the expression

$$\left(\frac{M^2 - 2}{M^2 - 1}\right)^2 \frac{\mu}{\sqrt{M^2 - 1}}$$

has been reduced to μ/M in Eq. (9) for $M >> 1$.

Equation (9) will be solved by the use of Galerkin's method. For a simply supported plate, the displacement function is assumed to be

$$W(\xi, \tau) = \sum_{n=1}^{\infty} u_n(\tau)\sin n\pi\xi \quad (10)$$

where n is a positive integer and defines the assumed vibration modes of the plate.

Substituting Eq. (10) into Eq. (9), yields

$$\frac{D_{11}}{D_{11}^{(0)}}\sum_n u_n(n\pi)^4\sin n\pi\xi + \frac{A_{11}h^2}{2D_{11}^{(0)}}\left\{\sum_m u_m^2\frac{(m\pi)^2}{2}\right\} \times \sum_n u_n(n\pi)^2\sin n\pi\xi + R_x\sum_n u_n(n\pi)^2\sin n\pi\xi + \sum_n \frac{d^2u_n}{d\tau^2}\sin n\pi\xi + \lambda\left[\sum_n u_n(n\pi)\cos n\pi\xi + \left(\frac{\mu}{\lambda M}\right)^{1/2}\sum_n \frac{du_n}{d\tau}\sin n\pi\xi\right] = P \qquad (11)$$

Multiplying both sides of Eq. (11) by $\sin s\pi\xi$ and integrating over the panel length, one obtains

$$\frac{D_{11}}{D_{11}^{(0)}}\frac{\pi^4u_s s^4}{2} + \frac{A_{11}h^2\pi^4}{8D_{11}^{(0)}}\left\{\sum_m m^2u_m^2\right\}u_s s^2 + \frac{R_x\pi^2u_s s^2}{2} + \frac{1}{2}\frac{d^2u_s}{d\tau^2} + \lambda\left\{\sum_n \frac{snu_n}{s^2-n^2}\times[1-(-1)^{s+n}] + \frac{1}{2}\left(\frac{\mu}{\lambda M}\right)^{1/2}\frac{du_s}{d\tau}\right\} = \frac{[1-(-1)^s]}{s\pi}P \qquad s = 1, \ldots, \infty \qquad (12)$$

Equation (12) represents a coupled set of second-order, nonlinear, ordinary differential equations for the determination of the time history of the modal amplitudes. The anisotropic properties of the two-dimensional composite plate are included in Eq. (12) through variables D_{11} and A_{11}. The general solution procedure of Eq. (12), in brief, is to specify D_{11}, A_{11}, R_x, λ, μ/M, P and to give an initial value of u_n and then to determine the u_n as function of time τ by the 12th-order Adams Predictor-Corrector numerical integration method. The time increment Δt is 0.0001.

Results and Discussions

The numerical integration process has been performed on a VAX-8600 high-speed computer. The composite material used in this study is Graphite/Epoxy AS-3002 with E_1/E_2 = 26.5, G_{12} = 1.184 E_2, and ν_{12} = 0.21. The symmetrically laminated angle-ply plate is composed of 10 layers of lamina, and the fiber angle of the top layer is defined as $+\theta$.

Convergence Study

When using series solutions, it is of importance to determine if sufficient terms are used in the analysis to obtain converged results. Figure 2 show the results of a convergence study for symmetric angle-ply plates with different fiber angles. The limit cycle oscillation amplitudes are plotted vs number of modes used. For small angle of fiber orientations (θ = 0 ~ 50 deg), four to five modes are sufficient to give accurate results. For larger fiber angles ($\theta \geq$ 60 deg), six to seven modes are needed. The modes required for convergence is also dependent on the magnitude of the aerodynamic pressure on the plate, as shown in Fig. 2. When θ = 70 deg, at low aerodynamic pressure (λ = 50 or 100), six modes is enough to obtain converged solution. However, at λ = 200 or higher, more modes are required.

In this study, six modes are used in all calculations. Satisfactory results are expected to be obtained for fiber angles larger than 60 deg since the aerodynamic pressure considered is low for $\theta > 60$ deg in order to keep the plate amplitude within certain range.

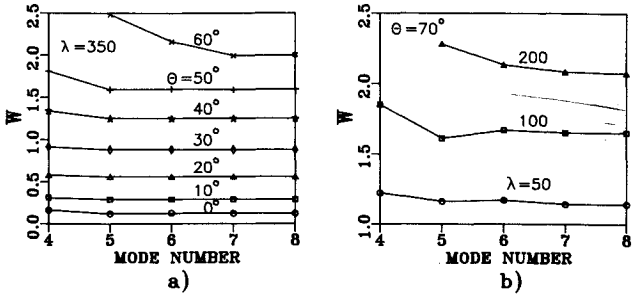

Fig. 2 Amplitude convergence study: ξ = 0.75; μ/M = 0.01.

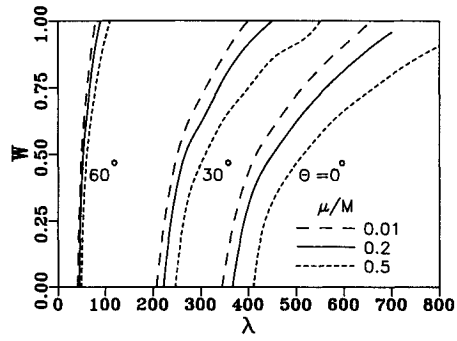

Fig. 3 Limit cycle amplitude vs dynamic pressure: ξ = 0.75.

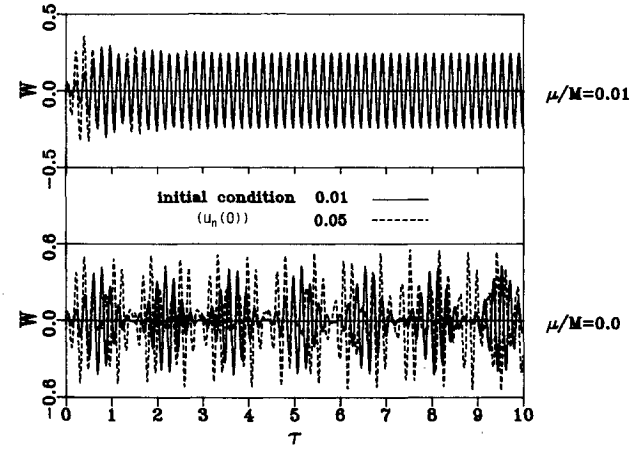

Fig. 4 Time history response of plate: θ = 10 deg; λ = 350; ξ = 0.75.

Effect of Aerodynamic Damping

The effect of aerodynamic damping on the plate amplitude of the limit cycle for different fiber orientations is given in Fig. 3. Aerodynamic damping has less effect on the oscillation amplitude as the fiber angle increases. However, for small fiber angles and high aerodynamic pressures, the aerodynamic damping has pronounced effect on the plate amplitude. Hence, for design purposes, the range of aerodynamic damping coefficient (or mass ratio) should be determined precisely in order to get lower amplitudes, which, in turn, give lower stresses in the plate. Nevertheless, the aerodynamic damping should be included in the numerical time integration analysis if the limit cycle oscillation is going to be reached. Figure 4 shows the time history responses of a 10-deg symmetric angle-ply plate with and without considering aerodynamic damping. It is clearly seen that the plate response without considering aerodynamic damping (by setting μ/M = 0) will never reach the limit cycle oscillation and is strongly dependent on the given initial condition (i.e., initial value of u_n at τ = 0). For the plate response including aerodynamic damping, the limit cycle is reached at τ = 4.0 and is independent of the form of the initial condition.

Effect of Fiber Orientation

The effects of fiber orientation on the amplitude and frequency (Hz) of the limit cycle oscillation are depicted in Figs. 5 and 6. As expected, the amplitudes increase with the dynamic pressure for all fiber orientations. However, due to the directional stiffness effect, i.e., rotating fibers away from the x axis results in a reduction of the plate stiffness in the x direction, the amplitude increasing rate is proportional to the fiber angle.

The frequency of the limit cycle oscillation increases with dynamic pressure for all fiber orientations. The reason is that the plate amplitude increases with the dynamic pressure, which, in turn, gives higher in-plane tensile stresses in the plate. Higher in-plane tensile stresses mean higher restoring forces in the plate, which make the plate vibrating faster. The increasing rate of the limit cycle frequency is about the same for all fiber orientations.

Effect of Elastic Modulus Ratio

Figure 7 shows the effect of the elastic modulus ratio on the amplitude of the limit cycle for different fiber angles. Increasing the modulus ratio increases the stiffness of the plate, which decreases the amplitude of oscillation. However, because the component of E_1/E_2 in the x direction becomes smaller as the fiber rotates away from the x axis, the reduction rate of the amplitude is smaller with a higher fiber angle.

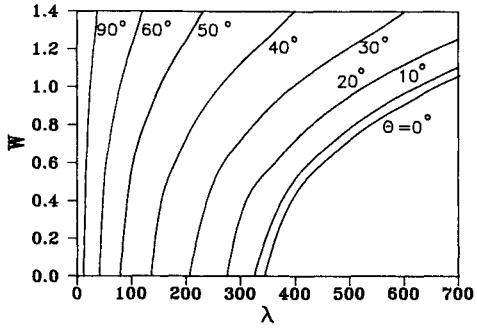

Fig. 5 Limit cycle amplitude vs dynamic pressure: $\xi = 0.75$; $\mu/M = 0.01$.

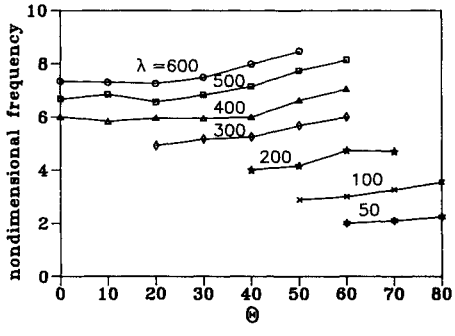

Fig. 6 Nondimensional frequency vs fiber angle: $\xi = 0.75$; $\mu/M = 0.01$.

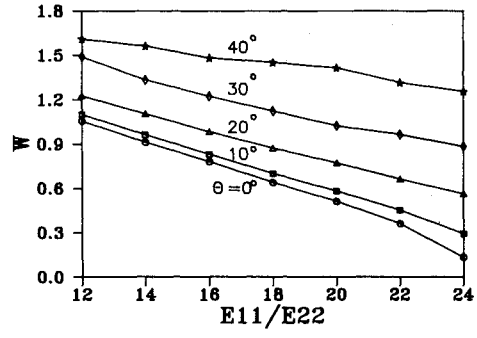

Fig. 7 Limit cycle amplitude vs modulus ratio: $\lambda = 350$; $\xi = 0.75$; $\mu/M = 0.01$.

Location of Maximum Amplitude of Limit Cycle

The maximum amplitude occurs at or near $x/a = 0.75$ for isotropic plates for most parameter combination cases.[1–11] However, the location of the maximum amplitude for composite laminate plates is a function of fiber angle and dynamic pressure, as shown in Fig. 8. The location of the maximum amplitude shifts from $x/a = 0.75$ toward the trailing edge of the plate as the fiber angle or dynamic pressure increases. For a fixed fiber orientation, say $\theta = 50$ deg, the shifting rate increases sharply as the dynamic pressure goes beyond a certain value. On the other hand, at a fixed dynamic pressure, say $\lambda = 350$, there is a rapid increase in x/a as the fiber angle goes higher than 40 deg.

Effect of Static Pressure Differential

The effect of static pressure differential can be seen easily from phase plane plots, as shown in Fig. 9. With the presence of static pressure differential, the whole phase diagram decreases in size and shifts toward the $+W$ direction. Also, the

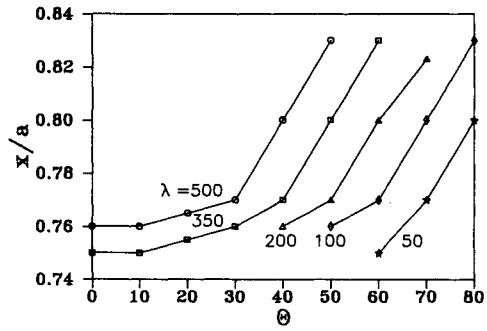

Fig. 8 Maximum amplitude location vs fiber angle: $\mu/M = 0.01$.

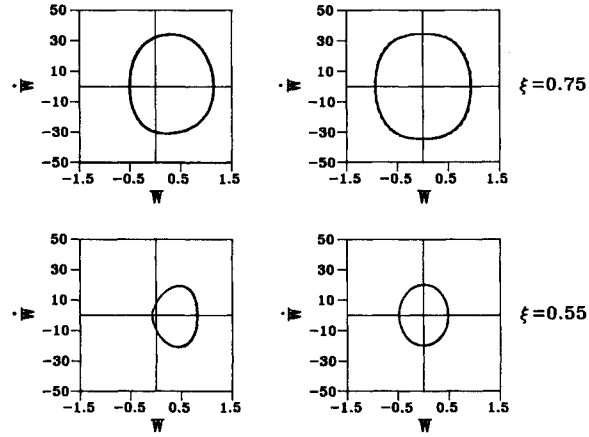

Fig. 9 Phase plane plot: $\theta = 20$ deg; $\lambda = 500$; $\mu/M = 0.01$.

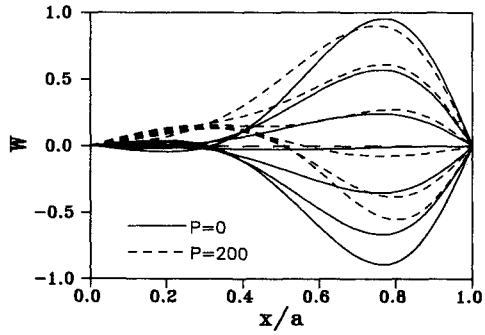

Fig. 10 Plate motion: $\theta = 20$ deg; $\lambda = 500$; $\mu/M = 0.01$.

phase diagram is no longer symmetry with respect to its mean steady equilibrium position.

Figure 10 illustrates the motion of the plate over a half cycle of oscillation for the cases with and without static pressure differential. For the case without static pressure differential, the plate motion is symmetric to its initial equilibrium position and the location of the maximum amplitude is always at $x/a = 0.77$. However, for a plate with static pressure differential, the plate motion is no longer symmetry with respect to either its initial equilibrium position or its mean steady equilibrium position, and the locatin of the maximum amplitude varies with time due to the presence of the static pressure. The effect of fiber orientation on the steady mean amplitudes $(W_s)_p$ [which is the location of vibration center, i.e., $(W_s)_p = \frac{1}{2}(W_{max} + W_{min})$] and the amplitudes of the oscillatory component $(W_d)_p$ [which is the amplitude measured from vibration center, i.e., $(W_d)_p = \frac{1}{2}(W_{max} - W_{min})$] are plotted in Figs. 11 and 12 for two different static pressure differentials. Although the steady mean amplitudes are almost in linear proportion to the static pressure differential for all fiber orientations, the steady mean amplitude curves are different. For θ varied from 0 to 20 deg, the steady mean amplitude curves are almost identical for both static pressure differential cases. When θ increases to 30 deg, the value of the maximum amplitude of $(W_s)_p$ remains the same as that of $\theta = 0$–20 deg, but the location moves from $x/a \cong 0.72$ to 0.57. With further increases in θ, the value

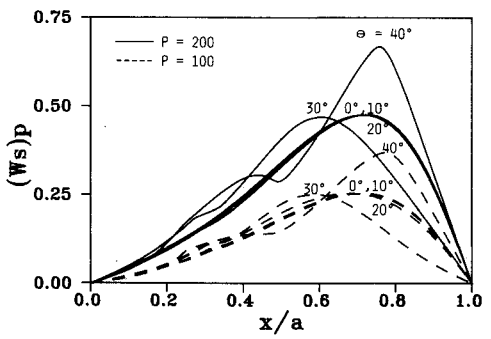

Fig. 11 Steady mean amplitude of the plate: $\lambda = 400$; $\mu/M = 0.01$.

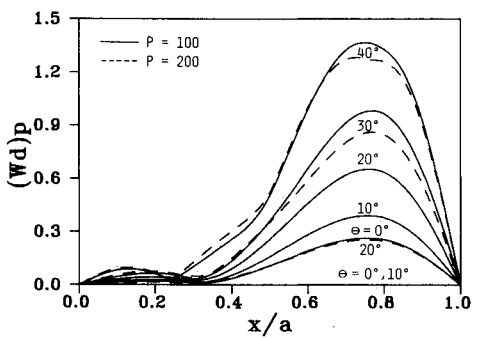

Fig. 12 Dynamic amplitude component of the plate: $\lambda = 400$; $\mu/M = 0.01$.

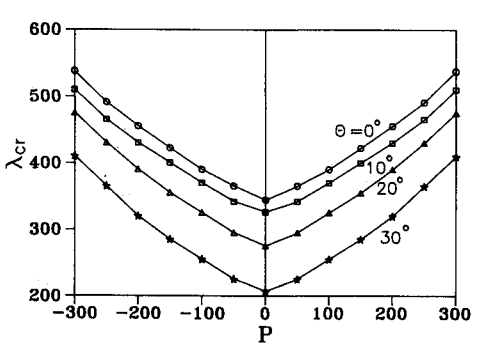

Fig. 13 Critical dynamic pressure vs static pressure differential: $\mu/M = 0.01$.

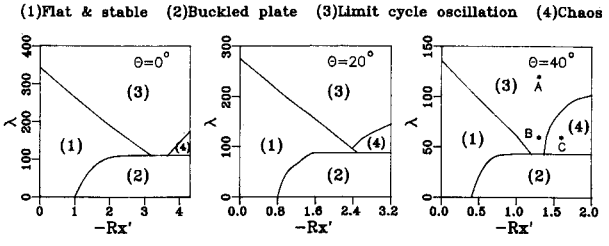

Fig. 14 Stability regions: $\xi = 0.75$; $\mu/M = 0.01$.

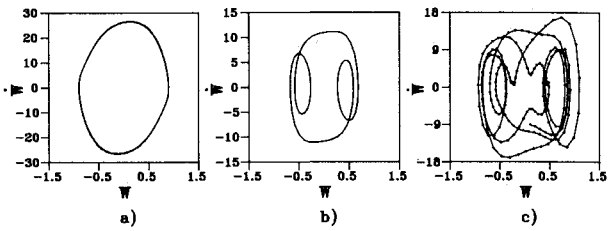

Fig. 15 Phase plane plot of points in Fig. 14.

of the maximum amplitude of $(W_s)_p$ jumps 50%, as compared to the cases of $\theta = 0$–30 deg, and its location moves back to $x/a \cong 0.78$. The amplitudes of the oscillatory component $(W_d)_p$ are, however, varied with θ and P. The amplitudes of $(W_d)_p$ for $P = 200$ are smaller than the case of $P = 100$ due to the presence of higher in-plane stresses induced by the higher static pressure differential. However, the amplitudes of $(W_d)_p$ for $P = 200$ are gradually closer to the value of $(W_d)_p$ for $P = 100$ as the fiber angle increases.

In Fig. 13, the stability boundary is shown in terms of λ_{cr} vs P for different fiber orientations. These values are determined when $(W_d)_p = 0$. The trend of λ_{cr} increasing with P is identical for all fiber angles.

Effect of In-Plane Loading

The effect of in-plane loading on the flutter boundaries was studied. The results plotted as dynamic pressure λ vs in-plane compression are shown in Fig. 14 for $\theta = 0$, 20, and 40 deg. For all θ values, the plate motion that may occur can be divided into four types: 1) for small λ and R_x, the plate remains stable and flat; 2) for small λ and moderate R_x, the plate buckles but is in dynamic stable situation; 3) for moderate λ and R_x, limit cycle oscillation occurs but with simple harmonic or subharmonic motion; and 4) for sufficiently high R_x and λ just above the boundary of the dynamic stable region, chaotic motion occurs.

The interesting cases are the limit cycle oscillation and chaotic motion. If the results are plotted in the phase plane, the distinctive type of motion that may occur can be seen easily. Figure 15 show three types of motion. The limit cycle with simple harmonic motion of point A in Fig. 14 is depicted in Fig. 15a. As the dynamic pressure drops from 120 to 60 and R_x remains unchanged, i.e., point B in Fig. 14, the limit cycle oscillation becomes a subharmonic motion, as shown in Fig. 15b. The larger orbit is the flutter motion and the two smaller orbits are associated with buckling. As the R_x is further increased, the motion becomes chaotic, as shown in Fig. 15c. The chaotic motion that occurs for certain parameter combinations of λ and R_x might be termed random. However, the minima and maxima of displacement and velocity of the motion are bounded in the phase plane.

Conclusions

The nonlinear flutter behavior of a two-dimensional composite laminated plate is demonstrated. The parameters studied include fiber orientation, elastic modulus ratio, aerodynamic damping, static pressure differential, and in-plane compressive load.

Based on the calculations, the following conclusions on the supersonic flutter characteristics of two-dimensional symmetric composite laminated plates can be made.

1) The aerodynamic damping has pronounced effect on the amplitude of limit cycle oscillation for small fiber angles and less effect for larger fiber angles.

2) Without the presence of in-plane loading and static pressure differential, the amplitude of limit cycle oscillation of the plate increases with the fiber angle. The amplitude increasing rate is also proportional to the fiber angle.

3) Increasing the elastic modulus ratio can reduce the oscillatory amplitude of the plate.

4) The oscillatory amplitude of the plate can be reduced with the presence of static pressure differential. However, the effect of static pressure differential on the oscillatory amplitude decreases with the increase of fiber angle.

5) With the presence of in-plane loading, the plate may have limit cycle oscillation or chaotic vibration depending on the magnitudes of fluid flow velocity and mechanical in-plane load. Slightly inereasing the in-plane load will change a subharmonic motion to chaotic motion.

References

[1]Dowell, E. H., "Nonlinear Oscillations of a Fluttering Plate," *AIAA Journal*, Vol. 4, No. 7, 1966, pp. 1267–1275.

[2]Dowell, E. H., "Nonlinear Oscillations of a Fluttering Plate II," *AIAA Journal*, Vol. 5, No. 10, 1967, pp. 1856–1862.

[3]Ventres, C. S., and Dowell, E. H., "Comparison of Theory and Experiment for Nonlinear Flutter of Loaded Plates," *AIAA Journal*, Vol. 8, No. 11, 1970, pp. 2022–2030.

[4]Eastep, F. E., and McIntosh, S. C., "Analysis of Nonlinear Panel Flutter and Response under Random Excitation or Nonlinear Aerodynamic Loading," *AIAA Journal*, Vol. 9, No. 3, 1971, pp. 411–418.

[5]Morino, L., "A Perturbation Method for Treating Nonlinear Panel Flutter Problems," *AIAA Journal*, Vol. 7, No. 3, 1969, pp. 405–411.

[6]Kuo, C. C., Morine, L., and Dingundji, J., "Perturbation and Harmonic Balance Methods for Nonlinear Panel Flutter," *AIAA Journal*, Vol. 10, No. 11, 1072, pp. 1479–1484.

[7]Smith, L., and Morino, L., "Stability Analysis of Nonlinear Differential Autonomous Systems with Applications to Flutter," *AIAA Journal*, Vol. 14, No. 3, 1976, pp. 333–341.

[8]Mei, C., "A Finite Element Approach for Nonlinear Panel Flutter," *AIAA Journal*, Vol. 15, No. 8, 1977, pp. 1107–1110.

[9]Rao, K. S., and Rao, G. V., "Large Amplitude Supersonic Flutter of Panels with Ends Elastically Restrained Against Rotation," *Computers and Structures*, Vol. 11, No. 3, 1980, pp. 197–201.

[10]Han, A. D., and Yang, T. Y., "Nonlinear Panel Flutter Using High-Order Triangular Finite Element," *AIAA Journal*, Vol. 21, No. 10, 1983, pp. 1453–1461.

[11]Sarma, B. S., and Varadan, T. K., "Nonlinear Panel Flutter by Finite Element Method," *AIAA Journal*, Vol. 26, No. 5, 1988, pp. 566–574.

[12]Dowell, E. H., "Flutter of a Buckled Plate as An Example of Chaotic Motion of A Deterministic Autonomous System," *Journal of Sound and Vibration*, Vol. 85, No. 3, 1982, pp. 333–344.

[13]Ketter, D. J., "Flutter of Flat Rectangular Orthotropic Panels," *AIAA Journal*, Vol. 5, No. 1, 1967, pp. 116–124.

[14]Rossettos, J. N., and Tong, P., "Finite Element Analysis of Vibration and Flutter of Cantilever Anisotropic Plates," *Journal of Applied Mechanics*, Vol. 41, No. 4, 1974, pp. 1075–1080.

[15]Sawyer, J. W., "Flutter and Buckling of General Laminated Plates," *Journal of Aircraft*, Vol. 14, No. 4, 1977, pp. 387–393.

[16]Shiau, L. C., Tsai, D. H., and Lee, L. J., "Finite Element Analysis of Composite Panel Flutter," *Third European Conference on Composite Materials*, Bordeaus, France, edited by A. R. Bunsell, P. Lamicq, and A. Massiah, Elsevier Applied Science, London, March 1989, pp. 341–346.

[17]Chia, C. Y., *Nonlinear Analysis of Plates*, McGraw-Hill, New York, 1980, p. 21.

[18]Jones, R. M., *Mechanics of Composite Materials*, Scripta, Washington DC, 1975, p. 51.